INTERNATIONAL JOURNAL FOR NUMERICAL METHODS IN FLUIDS
Int. J. Numer. Meth. Fluids 2000; **32**: 407–437

Simulation of transients in natural gas pipelines using hybrid TVD schemes

Junyang Zhou[a] and Michael A. Adewumi[b,*]

[a] *Petroleum and Natural Gas Engineering, The Pennsylvania State University, 128 Hosler Building, University Park, PA 16802, USA*
[b] *Petroleum and Natural Gas Section, Mineral Engineering Department, The Pennsylvania State University, 202 Hosler Building, University Park, PA 16802, USA*

SUMMARY

The mathematical model describing transients in natural gas pipelines constitutes a non-homogeneous system of non-linear hyperbolic conservation laws. The time splitting approach is adopted to solve this non-homogeneous hyperbolic model. At each time step, the non-homogeneous hyperbolic model is split into a homogeneous hyperbolic model and an ODE operator. An explicit 5-point, second-order-accurate total variation diminishing (TVD) scheme is formulated to solve the homogeneous system of non-linear hyperbolic conservation laws. Special attention is given to the treatment of boundary conditions at the inlet and the outlet of the pipeline. Hybrid methods involving the Godunov scheme (TVD/Godunov scheme) or the Roe scheme (TVD/Roe scheme) or the Lax–Wendroff scheme (TVD/LW scheme) are used to achieve appropriate boundary handling strategy. A severe condition involving instantaneous closure of a downstream valve is used to test the efficacy of the new schemes. The results produced by the TVD/Roe and TVD/Godunov schemes are excellent and comparable with each other, while the TVD/LW scheme performs reasonably well. The TVD/Roe scheme is applied to simulate the transport of a fast transient in a short pipe and the propagation of a slow transient in a long transmission pipeline. For the first example, the scheme produces excellent results, which capture and maintain the integrity of the wave fronts even after a long time. For the second example, comparisons of computational results are made using different discretizing parameters. Copyright © 2000 John Wiley & Sons, Ltd.

KEY WORDS: hybrid scheme; hyperbolic conservation laws; natural gas pipeline; non-homogeneous hyperbolic system; transient flow; TVD scheme; wave propagation

1. INTRODUCTION

Cost-effective design and operation of a gas transmission system require accounting for its response under unsteady or transient conditions. Actual operations invariably encounter transient states. The loss of a compressor, the addition or loss of supply or sale points,

* Correspondence to: Petroleum and Natural Gas Section, Mineral Engineering Department, The Pennsylvania State University, 202 Hosler Building, University Park, PA 16802-5000, USA. Tel.: + 1 814 8632816; fax: + 1 814 8631875.

CCC 0271–2091/2000/040407–31$17.50

Received 6 October 1995
Revised 16 July 1996

equipment malfunction, start-up and shutdown process and variable demands are just a few examples of the causes of pipeline transients.

Under isothermal conditions, the continuity and momentum equations, together with the equation of state, constitute the governing equations describing transient flow in natural gas pipelines. The assumptions usually made include isothermal flow, applicability of steady state friction and negligible wall expansion or contraction under pressure loads. For simulating transient flow of single-phase natural gas in pipelines, many previous investigators neglect the inertia term in the governing equations. This renders the resulting set of partial differential equations linear. Numerical methods previously used to solve this system of linear partial differential equations include the method of characteristics (MOC) and a variety of explicit and implicit finite difference schemes [1–4]. Neglecting the inertia term in the momentum equation will result in loss of accuracy of the simulation results. In order to compensate for the exclusion of the inertia term from the momentum equation, Yow [5] introduced the concept of *inertia multiplier* to partially account for the effect of the inertia term in the momentum equation. Wylie *et al.* [6] simulated transients in natural gas pipelines in accordance with the concept of the inertia multiplier. Rachford and Dupont [7] have demonstrated that calculations based on the concept of inertia multiplier will sometimes yield very misleading results. In the present study, the inertia term in the momentum equation is fully included. The governing equations, together with an equation of state, constitute a non-homogeneous hyperbolic system of first-order quasi-linear partial differential equations. The numerical solution of this set of non-homogeneous quasi-linear hyperbolic partial differential equations is not trivial.

First-order upwind schemes, derived from Steger and Warming's extension via flux splitting [8] of the Courant–Isaacson–Rees scheme [9] to non-linear hyperbolic systems usually lead to exceedingly viscous (dissipative) schemes, which tend to 'smear' non-stationary shocks and other discontinuities. The introduction by Lax–Wendroff [10], followed by MacCormack [11], of second-order centered schemes was accompanied, in spite of a substantial improvement in the overall accuracy, by the problem of damping or eliminating the oscillations that appear in the neighborhood of discontinuities [12]. This was done originally by introducing into the scheme an artificial viscosity term [13], which required a problem-dependent treatment, admittedly a rather awkward prerequisite for engineering applications.

Another approach is introducing a change of *monotonicity detector* [14,15], which can find the nodes where the monotonicity is broken and then trigger an efficient counter-measure, in the form of a flux limiter or slope limiter [14–16].

More recently, the concept of total variation diminishing (TVD) schemes introduced by Harten [17,18] extends ideas on monotonicity, which had been proposed for linear schemes by Godunov [19]. This has led to a wide range of first- and higher-order-accurate methods, which prove to be useful, both for theoretical and real engineering applications.

In the present study, an explicit, 5-point, second-order-accurate TVD scheme is formulated to solve the homogeneous part of a non-linear system of hyperbolic conservation laws describing transients in horizontal natural gas pipelines based on Harten's explicit, second-order-accurate TVD scheme [17]. Special attention is given to the numerical boundary conditions treatment at the inlet and at the outlet of the pipeline (i.e. the node 0 and nj respectively). Because the present explicit, second-order-accurate TVD scheme is a 5-point scheme, additional numerical schemes are needed for the two penultimate nodes (1 and $nj-1$).

The explicit, 3-point, first-order-accurate Godunov scheme, the explicit, 3-point, second-order Lax–Wendroff (LW) scheme, and the explicit, 3-point, first-order Roe scheme are used for this purpose. This results in hybrid TVD schemes, namely TVD/Godunov, TVD/LW and TVD/Roe schemes. For a test problem involving instantaneous closure of a downstream valve, the TVD/Roe and TVD/Godunov schemes produced excellent results, while the TVD/LW scheme performed reasonably well.

The TVD/Roe scheme is applied to simulate two field pipeline examples: (1) the transport of a fast transient in a short, 24 in. pipe, 300 ft long; (2) the propagation of a slow transient flow, with a 24 h cycle, in a 45 mile long, 8 in. inner diameter, transmission pipeline. For example (1), the TVD/Roe scheme produces excellent results, which capture and maintain the integrity of the wave fronts, even after a long time. The explicit, 3-point, first-order-accurate Godunov scheme also successfully produces the results; however, it loses accuracy with time. For example (2), comparisons of the computational results are made using different grid sizes, time steps and the Courant–Friedrich–Lewy (CFL)-like restrictions.

2. DEVELOPMENT OF THE MATHEMATICAL MODEL

For a pipeline with constant cross-sectional area, the one-dimensional continuity equation for natural gas flow is

$$\frac{\partial}{\partial t}(\rho) + \frac{\partial}{\partial x}(\rho u) = 0, \tag{1}$$

where ρ is the gas density, u is the gas velocity along the pipeline, x is the distance along the pipeline from pipeline inlet, and t is the time from the start of the time interval of interest.

The one-dimensional form of the momentum equation for gas flow in horizontal pipelines with constant temperature distribution along pipelines is given by

$$\frac{\partial}{\partial t}(\rho u) + \frac{\partial}{\partial x}(\rho u^2) = -\frac{\partial p}{\partial x} - \frac{f_g \rho u |u|}{2D}, \tag{2}$$

where p is the gas pressure, f_g is the friction factor for natural gas flow, and D is the internal diameter of the pipeline.

Writing the equation of state for natural gas as

$$p = \frac{ZRT}{M_g}\rho, \tag{3}$$

where Z is the natural gas compressibility factor, R is the universal gas constant, T is the absolute gas temperature, and M_g is the gas molecular weight.

Assuming isothermal flow conditions in the pipeline, the acoustic wave speed is given by

$$c = \left(\frac{ZRT}{M_g}\right)^{1/2}. \tag{4}$$

The steady state friction factor is used in the transient calculations, similar to conventional practice in the literature. The friction factor f_g can be calculated with the Chen's equation [20]. An average value of Z is used, and it is calculated from the Dranchuk and Abou-Kassem's method [21].

Setting $m = \rho u$ and substituting Equation (4) into Equation (3), Equations (1) and (2) may be rearranged as the following set of one-dimensional, first-order, non-linear hyperbolic partial differential equations for transient flows in horizontal natural gas pipelines:

$$\frac{\partial}{\partial t}\rho + \frac{\partial}{\partial x}m = 0, \tag{5}$$

$$\frac{\partial}{\partial t}m + \frac{\partial}{\partial x}\left(\frac{m^2}{\rho} + c^2\rho\right) = -\frac{f_g m|m|}{2D\rho}. \tag{6}$$

Equations (5) and (6) can be written in the following compact form:

$$\frac{\partial}{\partial t}\vec{U} + \frac{\partial}{\partial}\vec{F}(\vec{U}) = \vec{r}(\vec{U}), \tag{7}$$

where

$$\vec{U} = \begin{bmatrix} \rho \\ m \end{bmatrix}, \qquad \vec{F} = \begin{bmatrix} m \\ \dfrac{m^2}{\rho} + c^2\rho \end{bmatrix}, \qquad \vec{r}(\vec{U}) = \begin{bmatrix} 0 \\ -\dfrac{f_g m|m|}{2D\rho} \end{bmatrix}. \tag{8}$$

Equation (7) is the non-homogeneous hyperbolic model describing transients in horizontal natural gas pipelines.

3. CHARACTERISTIC EQUATIONS FOR THE NON-HOMOGENEOUS HYPERBOLIC MODEL

There are two distinct eigenvalues for the Jacobian matrix $A = (\partial/\partial\vec{U})\vec{F}(\vec{U})$, i.e.

$$a^1 = u - c, \qquad a^2 = u + c. \tag{9}$$

Following the method described by Hirsch [22], the characteristic equation C^- corresponding to the eigenvalue a^1 can be derived as

$$\frac{\partial \rho}{\partial t} - \frac{\rho}{c}\frac{\partial u}{\partial t} + (u - c)\left(\frac{\partial \rho}{\partial x} - \frac{\rho}{c}\frac{\partial u}{\partial x}\right) = \frac{\rho}{c}\frac{f_g u|u|}{2D}. \tag{10}$$

This can be written in the conservative variables as

$$\left(1 + \frac{m}{\rho c}\right)\frac{\partial \rho}{\partial t} - \frac{1}{c}\frac{\partial m}{\partial t} + \left(\frac{m}{\rho} - c\right)\left[\left(1 + \frac{m}{\rho c}\right)\frac{\partial \rho}{\partial x} - \frac{1}{c}\frac{\partial m}{\partial x}\right] = \frac{f_g m|m|}{2Dc\rho}. \tag{11}$$

The characteristic equation C^+ corresponding to the eigenvalue a^2 can also be derived as

$$\frac{\partial \rho}{\partial t} + \frac{\rho}{c}\frac{\partial u}{\partial t} + (u + c)\left(\frac{\partial \rho}{\partial x} + \frac{\rho}{c}\frac{\partial u}{\partial x}\right) = -\frac{\rho}{c}\frac{f_g u|u|}{2D}. \tag{12}$$

This can also be written in the conservative variables as

$$\left(1 - \frac{m}{\rho c}\right)\frac{\partial \rho}{\partial t} + \frac{1}{c}\frac{\partial m}{\partial t} + \left(\frac{m}{\rho} + c\right)\left[\left(1 - \frac{m}{\rho c}\right)\frac{\partial \rho}{\partial x} + \frac{1}{c}\frac{\partial m}{\partial x}\right] = -\frac{f_g m|m|}{2Dc\rho}. \tag{13}$$

4. THE INITIAL CONDITIONS

The solution of Equation (7) proceeds from specified initial field variable distributions, i.e. the distributions of gas density, ρ, and gas mass flux, $m = \rho u$, throughout the pipeline. In the absence of field data concerning the initial field variable distributions, it is assumed that steady state variable distributions comprise the initial conditions. These steady state distributions are obtained using an analytical equation [23], written as

$$\bar{\rho} = \frac{f_g m_0^2}{Dc^2\rho_0^2}\left(\frac{D}{f_g}\ln\bar{\rho} - \Delta L\right) + 1, \tag{14}$$

where

$$\bar{\rho} = \left(\frac{\rho}{\rho_0}\right)^2. \tag{15}$$

Equation (14), which is implicit in $\bar{\rho}$, is well suited for fixed-point iteration for determining density or pressure distributions.

5. FORMULATION OF THE NUMERICAL SCHEMES

5.1. Time splitting approach for non-homogeneous hyperbolic model

For the non-homogeneous hyperbolic model (7), the time splitting approach [24] is adopted to maintain the second-order accuracy of the complete scheme. At each time step, Equation (7) may be split into the following two subproblems:

$$\frac{\partial}{\partial t}\vec{U}+\frac{\partial}{\partial x}\vec{F}(\vec{U})=0, \tag{16}$$

$$\frac{\partial}{\partial t}\vec{U}=\vec{r}(\vec{U}). \tag{17}$$

Equation (16) is the source-free hyperbolic model, while Equation (17) is an ODE operator. The exact solution of Equation (17) is

$$\begin{bmatrix}\rho\\ m\end{bmatrix}=\begin{bmatrix}\tilde{\rho}\\ \dfrac{\tilde{m}}{1+\dfrac{f_g}{2D\tilde{\rho}}\Delta t|\tilde{m}|}\end{bmatrix}, \tag{18}$$

where $\tilde{U}=[\tilde{\rho}, \tilde{m}]^T$ is the solution of Equation (16) using the TVD scheme.

5.2. High resolution TVD scheme for homogeneous hyperbolic conservation laws

For reference purposes, a particular version of Harten's second-order-accurate, 5-point explicit TVD scheme for a one-dimensional homogeneous system of hyperbolic conservation laws is briefly described [17]. Consider a system of hyperbolic conservation laws of the form

$$\frac{\partial}{\partial t}U+\frac{\partial}{\partial x}f(U)=0, \tag{19}$$

where U is the vector of m conserved variables and f is the flux vector. The Jacobian matrix $A(U)=(\partial/\partial U)f(U)$ has real eigenvalues $(a^1, a^2, \ldots, a^m)$ and a complete set of right eigenvectors. Let $R=(R^1, R^2, \ldots, R^m)$ be a matrix whose columns are the right eigenvectors of A and let L be a matrix whose rows are the left eigenvectors of A.

Let $U_{j+1/2}=V(U_j, U_{j+1})$ denote an average of U_j and U_{j+1}, i.e. a smooth function $V(u, v)$ such that

$$V(u, v)=V(v, u), \tag{20}$$

$$V(u, u)=u, \tag{21}$$

and let $\alpha^k_{j+1/2}$ denote the component of $\Delta_{j+1/2}v=v_{j+1}-v_j$ in the co-ordinate system $\{R^k(v_{j+1/2})\}$

$$\Delta_{j+1/2}v=\sum_{k=1}^{m}\alpha^k_{j+1/2}R^k_{j+1/2}, \tag{22}$$

$$\alpha^k_{j+1/2}=L^k_{j+1/2}\Delta_{j+1/2}v. \tag{23}$$

Here we use the notation convention $b_{j+1/2}=b(v_{j+1/2})=b(V(v_j, v_{j+1}))$.

Then, one particular version of Harten's 5-point, second-order-accurate, explicit TVD scheme [17] can be written as follows:

$$v_j^{n+1} = v_j^n - \lambda(\tilde{f}_{j+1/2} - \tilde{f}_{j-1/2}), \tag{24}$$

$$\tilde{f}_{j+1/2} = \frac{1}{2}\left[f(v_j) + f(v_{j+1}) - \frac{1}{\lambda} \sum_{k=1}^{m} \beta_{j+1/2}^k R_{j+1/2}^k \right], \tag{25}$$

where

$$\beta_{j+1/2}^k = Q^k(v_{j+1/2}^k + \Upsilon_{j+1/2}^k)\alpha_{j+1/2}^k - (g_j^k + g_{j+1}^k), \tag{26}$$

$$v_{j+1/2}^k = \lambda a^k(v_{j+1/2}), \tag{27}$$

$$g_i^k = S_{i+1/2}^k \max[0, \min(|\tilde{g}_{i+1/2}^k|, \tilde{g}_{i-1/2}^k S_{i+1/2}^k)], \qquad S_{i+1/2}^k = \operatorname{sgn}(\tilde{g}_{i+1/2}^k), \tag{28}$$

$$\tilde{g}_{i+1/2}^k = \frac{1}{2}[Q^k(v_{i+1/2}^k) - (v_{i+1/2}^k)^2]\alpha_{i+1/2}^k, \tag{29}$$

$$\Upsilon_{i+1/2}^k = \frac{(g_{i+1}^k - g_i^k)}{\alpha_{i+1/2}^k}, \quad \text{when } \alpha_{i+1/2}^k \neq 0, \tag{30}$$

$$\Upsilon_{i+1/2}^k = 0, \quad \text{when } \alpha_{i+1/2}^k = 0.$$

Here $\lambda = \Delta t/\Delta x$.

Similarly, the second-order-accurate LW-type scheme and the first-order-accurate Godunov-type scheme are presented.

(1) The second-order-accurate LW-type scheme is obtained from (24) and (25) by defining

$$\beta_{j+1/2}^k = (v_{j+1/2}^k)^2 \alpha_{j+1/2}^k. \tag{31}$$

This is referred to as the LW scheme.

(2) The first-order-accurate Godunov-type scheme of Roe [17,25] is also obtained by defining β as follows:

$$\beta_{j+1/2}^k = |v_{j+1/2}^k| \alpha_{j+1/2}^k. \tag{32}$$

This is referred to as the Roe scheme.

It is worthwhile pointing out that in the formulation of Harten's 5-point, second-order-accurate, explicit TVD scheme, no particular form of averaging $V(u, v)$ (20) and (21) is required. Roe [25] uses a specific form of averaging that, on top of being mathematically

appealing, also enables the computational advantage of perfectly resolving stationary discontinuities. In all the schemes and experiments reported herein, the Roe linearization technique [25] is employed.

5.3. The Roe linearization technique for one-dimensional natural gas transients in pipelines

The mathematical model describing transient flows in natural gas pipelines is governed by Equations (7) and (8) or (9) and (10), which are the isothemmal one-dimensional Euler equations with wall friction. LeVeque [26] presented a Roe matrix for isothermal Euler equations of one-dimensional gas dynamics as follows:

$$\tilde{A}(v_\mathrm{l}, v_\mathrm{r}) = \begin{bmatrix} 0 & 1 \\ c^2 - \bar{u}^2 & 2\bar{u} \end{bmatrix}, \tag{33}$$

where the average velocity $\bar{u}$ has been defined by

$$\bar{u} = \frac{\rho_\mathrm{l}^{1/2} u_\mathrm{l} + \rho_\mathrm{r}^{1/2} u_\mathrm{r}}{\rho_\mathrm{l}^{1/2} + \rho_\mathrm{r}^{1/2}}. \tag{34}$$

This is often called the rho-averaged (or Roe-averaged) velocity. $\tilde{A}$ can be viewed as being the Jacobian matrix $(\partial/\partial \vec{U})\vec{F}(\vec{U})$ evaluated at the averaged velocity $\bar{u}$. The eigenvalues and eigenvectors of $\tilde{A}$ are given by

$$\tilde{a}^1 = \bar{u} - c, \qquad \tilde{a}^2 = \bar{u} + c, \tag{35}$$

$$\tilde{R}^1 = \begin{bmatrix} 1 \\ \bar{u} - c \end{bmatrix}, \qquad \tilde{R}^2 = \begin{bmatrix} 1 \\ \bar{u} + c \end{bmatrix}. \tag{36}$$

Let $\alpha^k(v_\mathrm{l}, v_\mathrm{r})$, $k = 1, 2$ be the solution of the following system of linear equations [see Equation (22)]:

$$v_\mathrm{r} - v_\mathrm{l} = \sum_{k=1}^{2} \alpha^k \tilde{R}^k(V(v_\mathrm{l}, v_\mathrm{r})). \tag{37}$$

Substituting Equation (36) into (37), then α^k in (37) are obtained by

$$\alpha^1 = \frac{1}{2c}\{-(m_\mathrm{r} - m_\mathrm{l}) + (\rho_\mathrm{r} - \rho_\mathrm{l})[\bar{u} + c]\}, \tag{38}$$

$$\alpha^2 = \frac{1}{2c}\{(m_\mathrm{r} - m_\mathrm{l}) - (\rho_\mathrm{r} - \rho_\mathrm{l})[\bar{u} - c]\}. \tag{39}$$

5.4. Formulation of the 5-point, second-order TVD scheme for the source-free hyperbolic model

In the formulation of the 5-point, second-order-accurate, explicit TVD scheme for the source-free hyperbolic model (16), the coefficient of numerical viscosity $Q^k(v)$ of Harten's 5-point, second-order, explicit TVD scheme [see Equations (24)–(30)] will be selected as

$$Q^k(v) = |v|. \tag{40}$$

Substituting Equations (34)–(36) and (38)–(40) into Harten's TVD scheme for general homogeneous hyperbolic systems of conservation laws [see Equations (24)–(30)], the second-order, 5-point, explicit TVD scheme for the source-free hyperbolic model (16) is given below.

$$\rho_j^{n+1} = \rho_j^n - \frac{\lambda}{2}(m_{j+1}^n - m_{j-1}^n) + \frac{1}{2}[(\beta_{j+1/2}^1 + \beta_{j+1/2}^2) - (\beta_{j-1/2}^1 + \beta_{j-1/2}^2)],$$
$$j = 2, 3, \ldots, nj-2, \tag{41}$$

$$m_j^{n+1} = m_j^n - \frac{\lambda}{2}\left\{\left[\frac{(m_{j+1}^n)^2}{\rho_{j+1}^n} + c^2\rho_{j+1}^n\right] - \left[\frac{(m_{j-1}^n)^2}{\rho_{j-1}^n} + c^2\rho_{j-1}^n\right]\right\}$$
$$+ \frac{1}{2}\{\{\beta_{j+1/2}^1[\bar{u}(v_{j+1/2}) - c] + \beta_{j+1/2}^2[\bar{u}(v_{j+1/2}) + c]\}$$
$$- \{\beta_{j-1/2}^1[\bar{u}(v_{j-1/2}) - c] + \beta_{j-1/2}^2[\bar{u}(v_{j-1/2}) + c]\}\}, \quad j = 2, 3, \ldots, nj-2, \tag{42}$$

where

$$\beta_{l+1/2}^k = |v_{l+1/2}^k + \Upsilon_{l+1/2}^k|\alpha_{l+1/2}^k - (g_l^k + g_{l+1}^k), \quad k = 1, 2; \quad l = j-1, j, \tag{43}$$

$$g_l^k = S_{l+1/2}^k \max[0, \min(|\tilde{g}_{l+1/2}^k|, \tilde{g}_{l-1/2}^k S_{l+1/2}^k)], \quad S_{l+1/2}^k = \operatorname{sgn}(\tilde{g}_{l+1/2}^k), \quad k = 1, 2;$$
$$l = j-1, j, j+1, \tag{44}$$

$$\tilde{g}_{l+1/2}^k = \frac{1}{2}[|v_{l+1/2}^k| - (v_{l+1/2}^k)^2]\alpha_{l+1/2}^k, \quad k = 1, 2; \quad l = j-2, j-1, j, j+1, \tag{45}$$

$$v_{l+1/2}^k = \lambda a^k(v_{l+1/2}), \quad k = 1, 2; \quad l = j-2, j-1, j, j+1, \tag{46}$$

$$\Upsilon_{l+1/2}^k = \frac{(g_{l+1}^k - g_l^k)}{\alpha_{l+1/2}^k}, \quad \text{when } \alpha_{l+1/2}^k \neq 0,$$

$$\Upsilon_{l+1/2}^k = 0, \quad \text{when } \alpha_{l+1/2}^k = 0, \quad k = 1, 2; \quad l = j-1, j, \tag{47}$$

$$a^1(v_{l+1/2}) = \bar{u}(v_{l+1/2}) - c, \quad l = j-2, j-1, j, j+1, \tag{48}$$

$$a^2(v_{l+1/2}) = \bar{u}(v_{l+1/2}) + c, \quad l = j-2, j-1, j, j+1, \tag{49}$$

$$\bar{u}(v_{l+1/2}) = \frac{\sqrt{\rho_l^n}u_l^n + \sqrt{\rho_{l+1}^n}u_{l+1}^n}{\sqrt{\rho_l^n} + \sqrt{\rho_{l+1}^n}}, \quad l = j-2, j-1, j, j+1, \tag{50}$$

$$\alpha_{l+1/2}^1 = \frac{1}{2c}\{-(m_{l+1}^n - m_l^n) + (\rho_{l+1}^n - \rho_l^n)[\bar{u}(v_{l+1/2}) + c]\}, \quad l = j-2, j-1, j, j+1, \tag{51}$$

$$\alpha_{l+1/2}^2 = \frac{1}{2c}\{(m_{l+1}^n - m_l^n) - (\rho_{l+1}^n - \rho_l^n)[\bar{u}(v_{l+1/2}) - c]\}, \quad l = j-2, j-1, j, j+1. \tag{52}$$

Here $u_l^n = m_l^n/\rho_l^n$ and $\lambda = \Delta t/\Delta x$.

5.5. Numerical treatment of boundary conditions

Physical boundary conditions at the inlet and outlet of pipelines will be imposed to allow the consideration of a wide variety of field situations. The physical boundary conditions fall into two categories: (1) the inlet natural gas density (or pressure) is maintained at a constant value (or a known function of time), while the outlet mass flux is a known function of time (or a constant value); (2) both the inlet and outlet mass fluxes are some known functions of time respectively. These are all the boundary conditions required by the governing equations (5) and (6) or (7) and (8). In addition to physical boundary conditions required by the governing equations, numerical boundary conditions at the inlet and outlet are required by the finite difference schemes.

The characteristic boundary method, the first-order and second-order space extrapolation methods, and a one-sided first-order difference method [29–31] are tested as the numerical boundary conditions handling strategies. The finite difference equations developed for the treatments of boundary conditions in each case are described below.

(1a) If the inlet natural gas density (or pressure) remains constant or is a known function of time, then the finite difference equation at the inlet of the pipeline for the gas mass flux may be written as follows:

Characteristic boundary method:

$$m_0^{n+1} = m_0^n - \frac{\Delta t}{\Delta x}\left(c - \frac{m_0^n}{\rho_0^n}\right)\left[\left(c + \frac{m_0^n}{\rho_0^n}\right)(\rho_1^n - \rho_0^n) - (m_1^n - m_0^n)\right] - \frac{f_g}{2D}\frac{m_0^n|m_0^n|}{\rho_0^n}\Delta t + \left(c + \frac{m_0^n}{\rho_0^n}\right)(\rho_0^{n+1} - \rho_0^n). \tag{53}$$

First-order space extrapolation:

$$m_0^{n+1} = m_1^{n+1}. \tag{54}$$

Second-order space extrapolation:

$$m_0^{n+1} = 2m_1^{n+1} - m_2^{n+1}. \tag{55}$$

One-sided first-order difference method:

$$m_0^{n+1} = m_0^n - \frac{\Delta t}{\Delta x}\left[\left(\frac{(m_1^n)^2}{\rho_1^n} + c^2\rho_1^n\right) - \left(\frac{(m_0^n)^2}{\rho_0^n} + c^2\rho_0^n\right)\right] - \frac{f_g}{2D}\frac{m_0^n|m_0^n|}{\rho_0^n}\Delta t. \tag{56}$$

(1b) If the inlet mass flux is constant or a known function of time, then the finite difference equation at the inlet of the pipeline for the gas density may be written as below:

Characteristic boundary method:

$$\rho_0^{n+1} = \rho_0^n + \frac{\Delta t}{\Delta x}(m_0^n - m_1^n)\frac{1 - \dfrac{m_0^n}{c\rho_0^n}}{1 + \dfrac{m_0^n}{c\rho_0^n}} - \frac{\Delta t}{\Delta x}(\rho_1^n - \rho_0^n)\left(\frac{m_0^n}{\rho_0^n} - c\right) + \frac{m_0^{n+1} - m_0^n}{c + \dfrac{m_0^n}{\rho_0^n}} + \frac{f_g m_0^n|m_0^n|\Delta t}{2D\rho_0^n\left(c + \dfrac{m_0^n}{\rho_0^n}\right)}. \tag{57}$$

First-order space extrapolation:

$$\rho_0^{n+1} = \rho_1^{n+1}. \tag{58}$$

Second-order space extrapolation:

$$\rho_0^{n+1} = 2\rho_1^{n+1} = \rho_2^{n+1}. \tag{59}$$

One-sided first-order difference method:

$$\rho_0^{n+1} = \rho_0^n + \frac{\Delta t}{\Delta x}(m_0^n - m_1^n). \tag{60}$$

(2) If the outlet mass flux is a constant value or a known function of time, then the finite difference equation at the outlet of the pipeline for the gas density may be written as follows:

Characteristic boundary method:

$$\rho_{nj}^{n+1} = \rho_{nj}^{n} + \frac{\Delta t}{\Delta x}(m_{nj-1}^{n} - m_{nj}^{n}) \frac{1 + \dfrac{m_{nj}^{n}}{c\rho_{nj}^{n}}}{1 - \dfrac{m_{nj}^{n}}{c\rho_{nj}^{n}}} - \frac{\Delta t}{\Delta x}(\rho_{nj}^{n} - \rho_{nj-1}^{n})\left(\frac{m_{nj}^{n}}{\rho_{nj}^{n}} + c\right) - \frac{m_{nj}^{n+1} - m_{nj}^{n}}{c - \dfrac{m_{nj}^{n}}{\rho_{nj}^{n}}}$$
$$- \frac{f_g m_{nj}^{n} |m_{nj}^{n}| \Delta t}{2D\rho_{nj}^{n}\left(c - \dfrac{m_{nj}^{n}}{\rho_{nj}^{n}}\right)}. \tag{61}$$

First-order space extrapolation:

$$\rho_{nj}^{n+1} = \rho_{nj-1}^{n+1}. \tag{62}$$

Second-order space extrapolation:

$$\rho_{nj}^{n+1} = 2\rho_{nj-1}^{n+1} - \rho_{nj-2}^{n+1}. \tag{63}$$

One-sided first-order difference method:

$$\rho_{nj}^{n+1} = \rho_{nj}^{n} + \frac{\Delta t}{\Delta x}(m_{nj-1}^{n} - m_{nj}^{n}), \tag{64}$$

where the subscripts 0 and *nj* denote values at node 0 and *nj* respectively, i.e. the inlet and outlet of the pipeline.

5.6. Numerical schemes for the two penultimate nodes (1 and nj − 1) when using TVD method

Since the second-order, explicit TVD scheme is a 5-point scheme rather than a 3-point scheme, special schemes are needed for the two penultimate grid nodes (1 and $nj-1$). Usually, researchers have implemented first-order space extrapolation method to handle these two penultimate nodes (e.g. Yee *et al.* [27]). In the present study, hybrid methods involving the 3-point, first-order-accurate, explicit Godunov scheme (TVD/Godunov scheme), or the 3-point, first-order-accurate, explicit Roe scheme (TVD/Roe scheme) or the 3-point, second-order, explicit Lax–Wendroff scheme (TVD/LW scheme) are used to achieve appropriate boundary scheme handling strategy. These methods are presented below.

5.6.1. Hybrid method involving the 3-point, first-order-accurate, explicit Godunov scheme. The first-order, 3-point, explicit Godunov scheme [12,19] for the homogeneous hyperbolic model (16) can be written as

$$\vec{U}_{j+1/2}^{n+1} = \frac{1}{2}(\vec{U}_{j+1}^{n} + \vec{U}_{j}^{n}) - \frac{\Delta t}{\Delta x}(\vec{F}_{j+1}^{n} - \vec{F}_{j}^{n}), \tag{65}$$

$$\vec{U}_{j}^{n+1} = \vec{U}_{j}^{n} - \frac{\Delta t}{\Delta x}(\vec{F}_{j+1/2}^{n+1} - \vec{F}_{j-1/2}^{n+1}). \tag{66}$$

By expanding Equations (65) and (66), the numerical boundary scheme for the homogeneous hyperbolic model (16) at nodes 1 and $nj-1$, which is described by the 3-point, first-order-accurate, explicit Godunov scheme, can be written as

$$\rho_{j+1/2}^{n+1} = \frac{1}{2}(\rho_{j+1}^{n} + \rho_{j}^{n}) - \frac{\Delta t}{\Delta x}(m_{j+1}^{n} - m_{j}^{n}), \quad j = 0, 1, nj-2, nj-1, \tag{67}$$

$$m_{j+1/2}^{n+1} = \frac{1}{2}(m_{j+1}^{n} + m_{j}^{n}) - \frac{\Delta t}{\Delta x}\left[\frac{(m_{j+1}^{n})^2}{\rho_{j+1}^{n}} + c^2\rho_{j+1}^{n} - \left(\frac{(m_{j}^{n})^2}{\rho_{j}^{n}} + c^2\rho_{j}^{n}\right)\right],$$
$$j = 0, 1, nj-2, nj-1, \tag{68}$$

$$\rho_{j}^{n+1} = \rho_{j}^{n} - \frac{\Delta t}{\Delta x}(m_{j+1/2}^{n+1} - m_{j-1/2}^{n+1}), \quad j = 1, nj-1, \tag{69}$$

$$m_{j}^{n+1} = m_{j}^{n} - \frac{\Delta t}{\Delta x}\left[\frac{(m_{j+1/2}^{n+1})^2}{\rho_{j+1/2}^{n+1}} + c^2\rho_{j+1/2}^{n+1} - \left(\frac{(m_{j-1/2}^{n+1})^2}{\rho_{j-1/2}^{n+1}} + c^2\rho_{j-1/2}^{n+1}\right)\right], \quad j = 1, nj-1, \tag{70}$$

5.6.2. Hybrid method involving the 3-point, first-order accurate, explicit Roe scheme. The Roe scheme is used for the two penultimate grid nodes (1 and $nj-1$) while solving the source-free hyperbolic model (16). This may be expressed by Equations (41), (42), (46) and (48)–(52), with $j = 1, nj-1$ and

$$\beta_{l+1/2}^{k} = |v_{l+1/2}^{k}|\alpha_{l+1/2}^{k}, \quad k = 1, 2; \quad l = j-1, j. \tag{71}$$

5.6.3. Hybrid method involving the 3-point, second-order-accurate, explicit LW scheme. The numerical scheme for the two penultimate grid nodes (1 and $nj-1$), which is described by the 3-point, second-order-accurate, explicit LW scheme, can be expressed by Equations (41), (42), (46) and (48)–(52), with $j = 1, nj-1$ and

$$\beta_{j+1/2}^{k} = (v_{j+1/2}^{k})^2\alpha_{j+1/2}^{k}, \quad k = 1, 2; \quad l = j-1, j. \tag{72}$$

A severe condition, involving instantaneous downstream valve closure will be used to test the efficacy of these new second-order-accurate, explicit hybrid TVD schemes. In spite of the strong wave generated, these schemes successfully handle the problem.

6. NUMERICAL EXPERIMENTS AND COMPARISONS

Three examples are simulated using both the first-order explicit Godunov scheme and the second-order explicit hybrid TVD schemes. The first is a test problem of instantaneous closure of a downstream valve; the second is the transport of a fast transient in a 300 ft long, 24 in. inner diameter short pipeline; and the last is the propagation of a slow transient flow, with a 24 h cycle, in a 45 mile long, 8 in. inner diameter transmission pipeline.

6.1. Test problem 1: instantaneous closure of downstream valve

A severe condition, involving instantaneous downstream valve closure will be used to test the efficacy of the numerical treatments of the boundary conditions at inlet and outlet of the pipeline for both the first-order-accurate, explicit Godunov scheme and the second-order-accurate, explicit hybrid TVD schemes. Included in these are TVD/Godunov, TVD/Roe and TVD/LW schemes. The test problem is hereby stated. At $t = 0^-$, steady state flow is established (pipeline length and diameter are 30 m and 0.1 m respectively) with gas mass flux of 20 kg m^{-2} s^{-1} and inlet gas density of 2 kg m^{-3}; at $t = 0^+$, the downstream valve is closed instantaneously, thus setting the gas mass flux at the outlet equal to zero, while the inlet mass flux is maintained at its original value. The isothermal sound speed is set at 360 m s^{-1}, and the wall friction factor is 0.03.

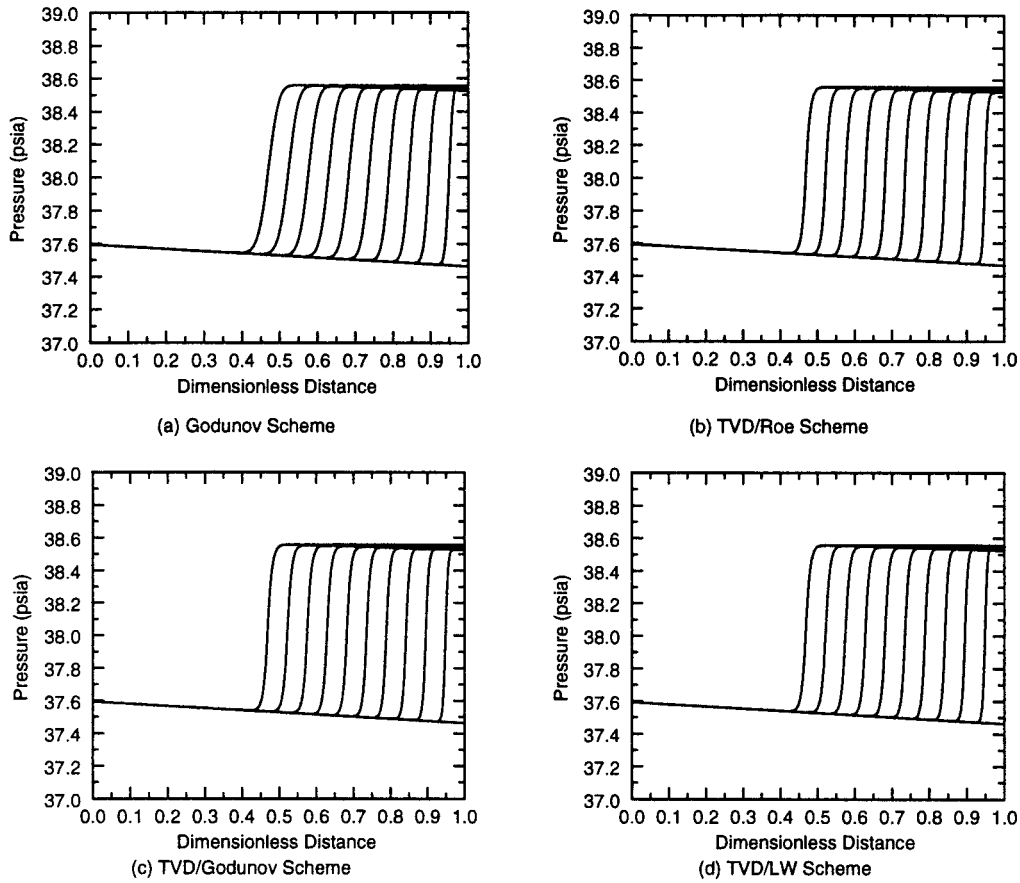

Figure 1. The predicted pressure wave propagation for test problem 1 (characteristic boundary treatment).

Figure 1 shows the predicted pressure wave propagation by the Godunov scheme, the TVD/Roe scheme, the TVD/Godunov scheme and the TVD/LW scheme with characteristic boundary treatment (see Equations (57) and (61)). Figure 2 shows the predicted gas mass flux wave propagation. Figure 3 shows the predicted gas velocity wave propagation. In all the numerical experiments, the grid size $\Delta x = 0.1$ m, the time step $\Delta t = 0.1$ ms, the CFL number $\mathrm{CFL} = 0.36$ and the time interval between two neighboring wave fronts $\Delta T = 4.5$ ms. These results demonstrate that the characteristic numerical boundary treatment is successful for both the first-order Godunov scheme and the second-order hybrid TVD schemes. They have the capability of capturing wave fronts without oscillations. For the appropriate numerical boundary scheme handling strategy, both the hybrid TVD/Godunov and TVD/Roe schemes produce excellent results without wave fronts oscillations, while the hybrid TVD/LW scheme

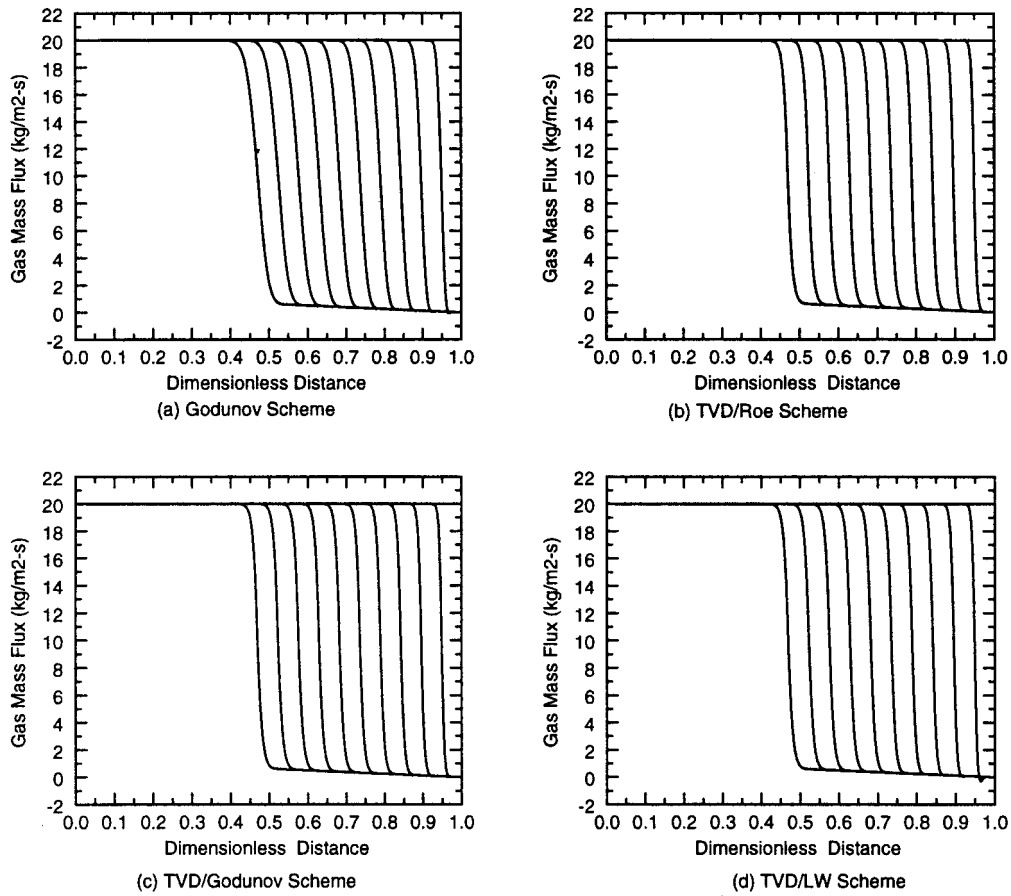

Figure 2. The predicted gas mass flux wave propagation for test problem 1 (characteristic boundary treatment).

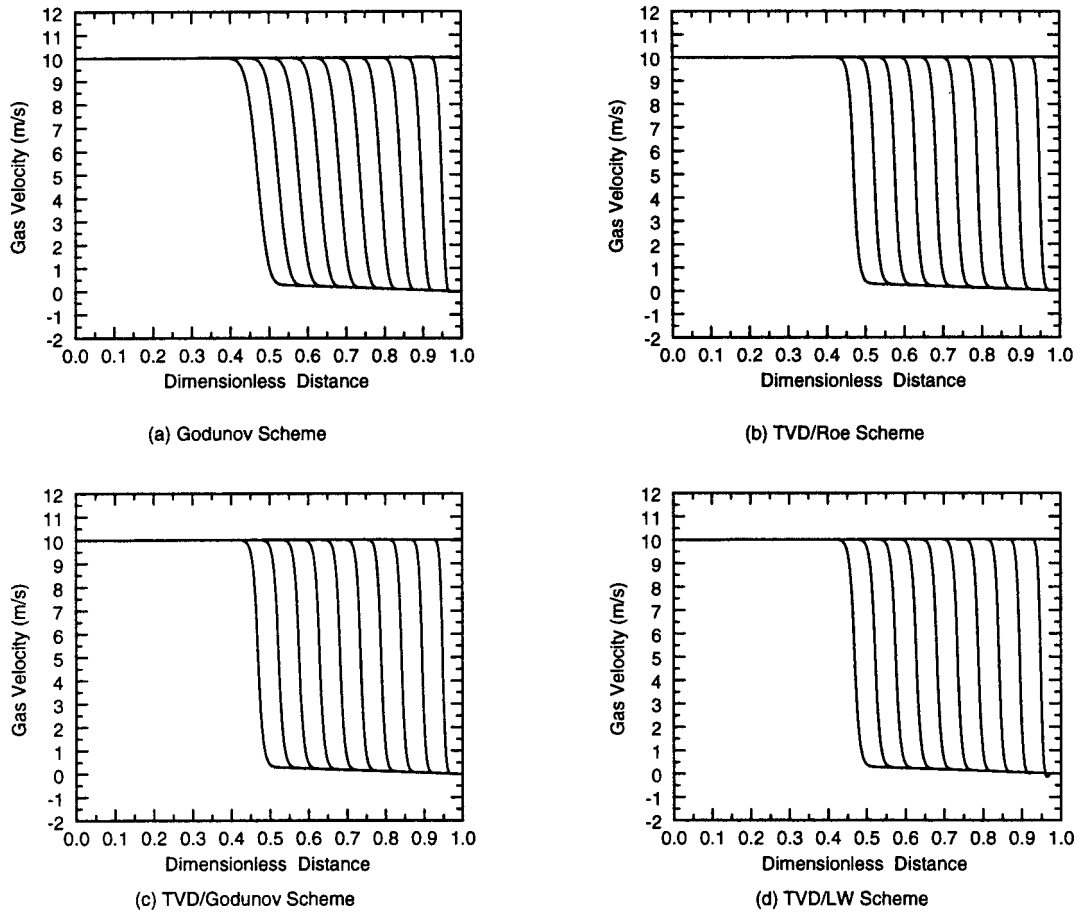

Figure 3. The predicted gas velocity wave propagation for test problem 1 (characteristic boundary treatment).

performs reasonably well with very slight wave front oscillations in the gas mass flux and gas velocity wave predictions.

Figure 4 compares the performance of the first-order accurate Godunov scheme and the second-order accurate hybrid TVD/Godunov scheme with characteristic boundary treatment (see Equations (57) and (61)) by the prediction of pressure wave and gas mass flux wave propagation and reflection in the pipeline. The pertinent parameters in Figure 4 are the same as those in Figures 1–3. It can be observed that the second-order hybrid TVD/Godunov scheme captures sharper wave fronts (pressure wave in Figure 4(a) and gas mass flux wave in Figure 4(b)) than the first-order Godunov scheme.

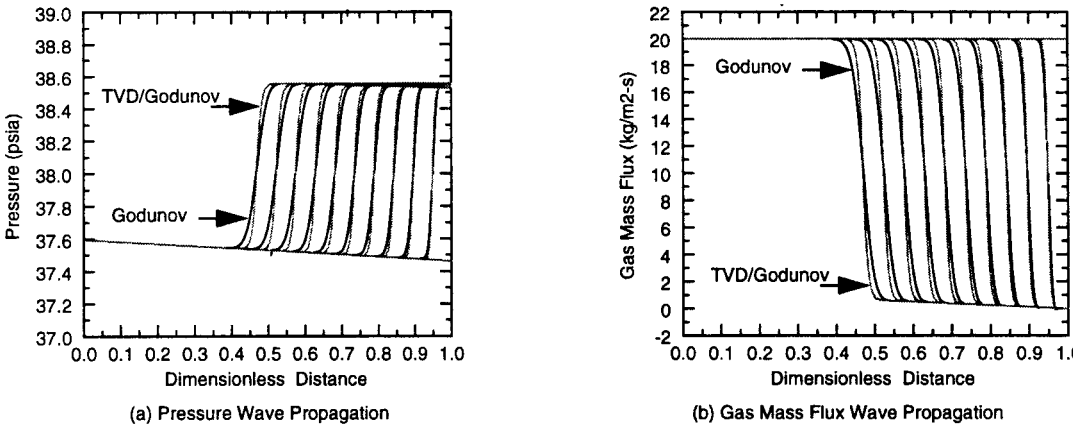

Figure 4. Comparison of Godunov scheme and TVD/Godunov scheme for test problem 1 (characteristic boundary treatment).

Figures 5–7 show the performance of four different numerical boundary condition treatment strategies for each of the three different hybrid TVD schemes (TVD/Roe, TVD/Godunov and TVD/LW) respectively. All the pertinent parameters in these figures are the same as those in Figures 1–4. Figure 5 shows the predicted gas mass flux wave propagation using the hybrid TVD/Roe scheme with four different numerical boundary treatment strategies. The following conclusions can be drawn from Figure 5 for the hybrid TVD/Roe scheme: (1) the characteristic numerical boundary method produces the best result (a similar conclusion has been drawn by Chu and Sereny [28]); (2) the first-order space-extrapolation method still produces good results in this case; (3) the second-order space extrapolation method and the one-sided first-order difference method are not as good as the characteristic numerical boundary method and the first-order space-extrapolation method (a similar conclusion has been drawn by Chu and Sereny [28]); they produce comparable results which have slight wave fronts oscillations near the downstream valve at the very first time. These conclusions can also be drawn for the hybrid TVD/Godunov scheme (Figure 6). For the hybrid TVD/LW scheme (Figure 7), all the numerical boundary condition treatment strategies cannot eliminate wave fronts oscillations. However, conclusions (1) and (3) still hold for the hybrid TVD/LW scheme in terms of the wave fronts oscillations.

6.2. Test problem 2: fast transient in a short pipe

The transport of a fast transient in a short gas pipe with an impulse supply of gas mass flux at the inlet of the pipe is simulated using both the Godunov and the TVD/Roe schemes. A pipeline 300 ft (91.44 m) long and 24 in. (0.6096 m) in diameter is initially packed to 600 psi along the pipeline with no flow. At $t = 0^+$, the upstream inflow begins to increase linearly and reaches 600 MMCF/D at 0.145 s, then decreases linearly to zero again at 0.29 s, and then remains constant at zero. The downstream end is closed. The friction factor is 0.03, and the isothermal sound wave speed is 1142 ft s^{-1} (348 m s^{-1}).

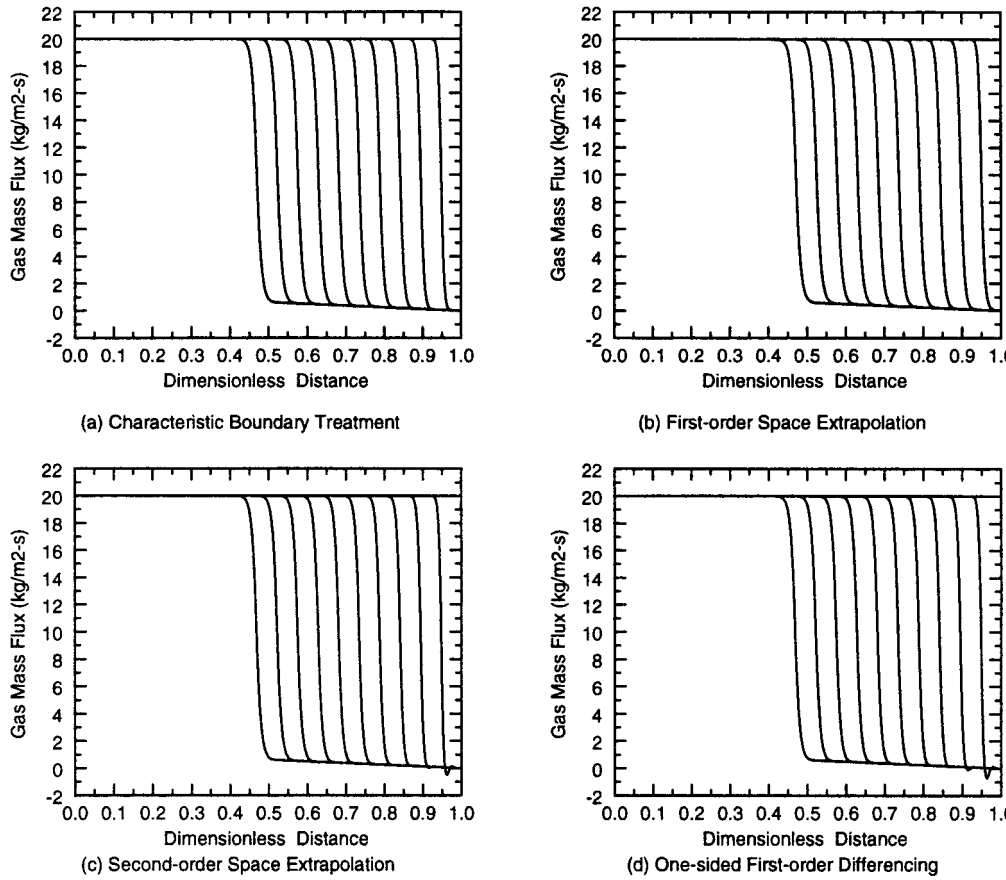

Figure 5. TVD/Roe scheme with different numerical boundary condition treatments for test problem 1 (gas mass flux wave propagation).

Figure 8 shows the predicted pressure wave propagation using both the first-order Godunov scheme and the second-order TVD/Roe scheme with the characteristic numerical boundary treatment (see Equations (57) and (61)). For the calculation of the first-order Godunov scheme, the grid size, $\Delta x = 0.9144$ m (100 mesh elements), the time step, $\Delta t = 0.09144$ ms, hence CFL $= 0.0348$; for the second-order hybrid TVD/Roe scheme, the same grid size was used but the time step size is 10 times that for the Godunov scheme ($\Delta t = 0.9144$ ms, CFL $= 0.348$). In both cases, the time interval between two neighboring fronts is $\Delta T = 22.86$ ms. It can be seen that during the initial period of 0.25146 s, both schemes produce similar results, which completely capture the wave fronts.

In Figures 9–11, the discretizing parameters are the same as those in Figure 8 for both the Godunov and the hybrid TVD/Roe schemes. Figure 9 shows the predicted pressure histories

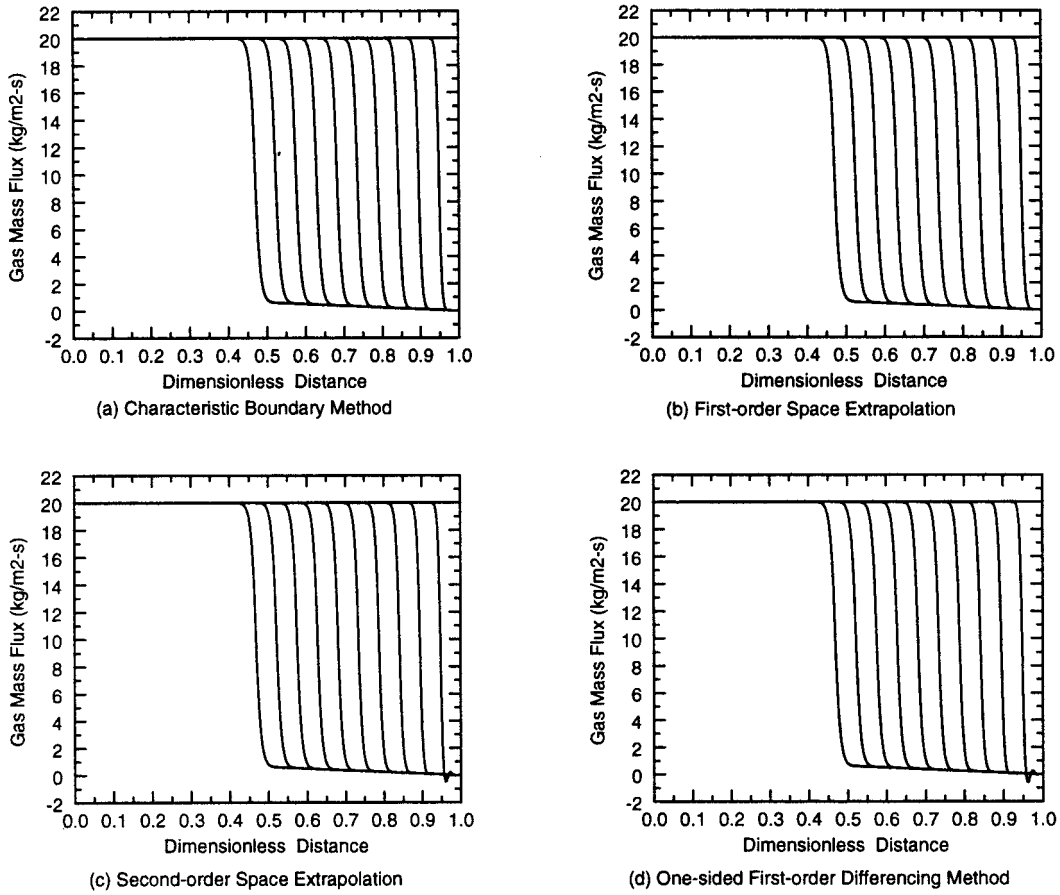

Figure 6. TVD/Godunov scheme with different numerical boundary condition treatments for test problem 1 (gas mass flux wave propagation).

at the inlet for the time interval of 0–23 s. It can be observed that initially, the pressure peak at the inlet increases with time, mainly due to the interaction between the pressure wave propagation and reflection along the pipeline; subsequently, the pressure peak decreases with time, mainly due to the dissipation nature of the flow system. Figure 10 shows a better resolution of the predicted pressure histories at the inlet for the time interval of 0–2.4 s, while Figure 11 shows the predicted pressure histories at the inlet for the time interval of 20–23 s. Using the first-order Godunov scheme, the pressure wave fronts are maintained and captured during the first 0.8 s. During the period of 0.8–2.4 s, there are some slight overshoots around the wave front. After that, the pressure wave fronts are resolved but with loss of accuracy. On the other hand, with the second-order hybrid TVD/Roe scheme, the integrity of the pressure wave fronts have been captured and maintained within the total time interval of 0–23 s, which

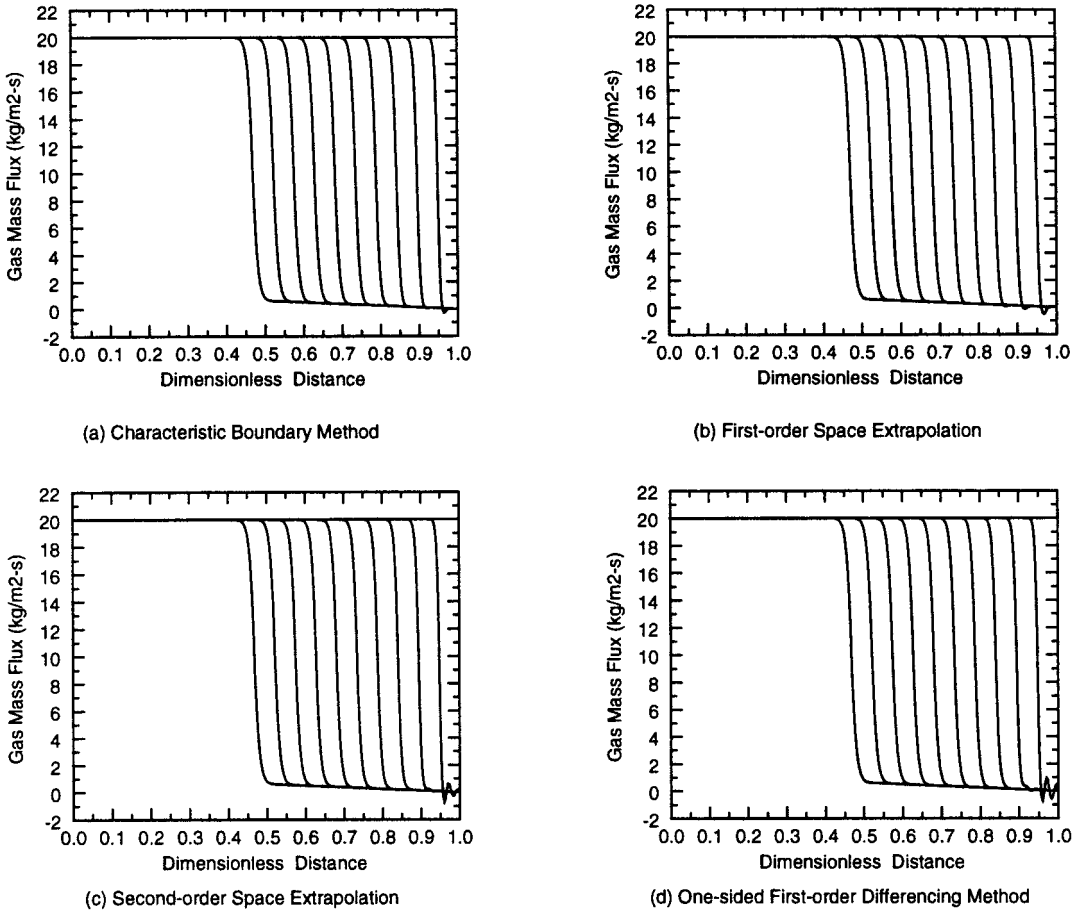

Figure 7. TVD/LW scheme with different numerical boundary condition treatments for test problem 1 (gas mass flux wave propagation).

indicates that the hybrid TVD scheme provides significant advantage over the explicit Godunov scheme.

6.3. Test problem 3: slow transient in a long transmission pipeline

The propagation of a slow transient flow in an actual field transmission pipeline is simulated using the TVD/Roe scheme with one-sided first-order difference method for the treatment of numerical boundary conditions (see Equations (56) and (64)). The system is an 8.15 in. inner diameter, 44.9 mile long pipeline transporting natural gas with a specific gravity of 0.675 at a temperature of 50°F. The gas dynamic viscosity μ_g is 7.957×10^{-6} lbm ft^{-1} s^{-1}, while the roughness of the pipeline wall ε is 0.024300 in. Due to the lack of initial field variable

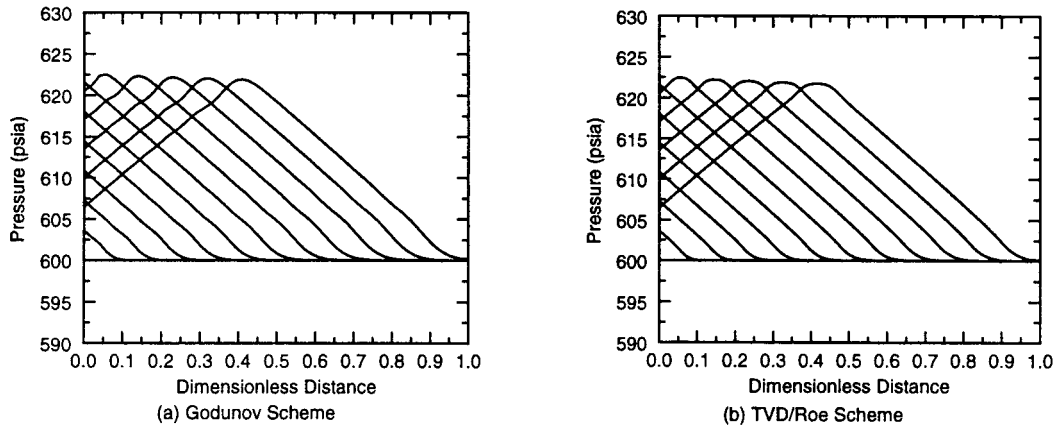

Figure 8. Predicted pressure wave propagation along pipeline for test problem 2.

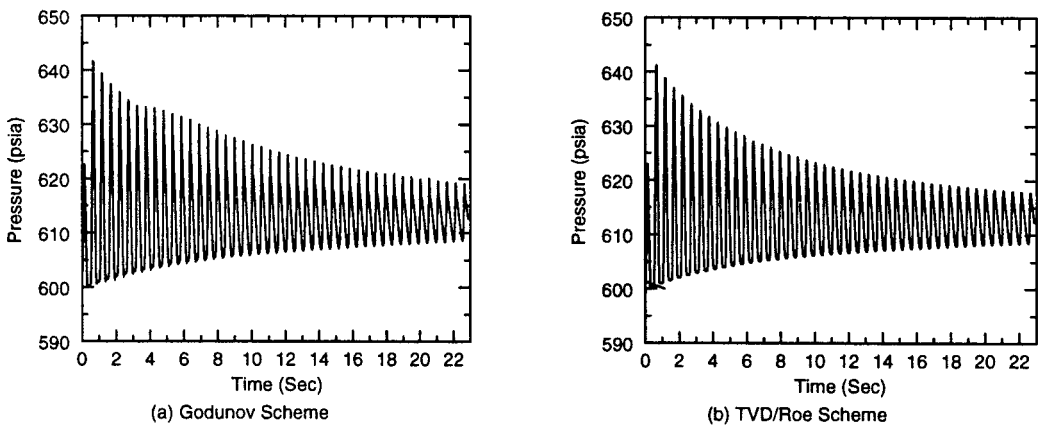

Figure 9. Predicted pressure histories at the inlet for test problem 2.

distribution data, the steady state field variable distributions are imposed as the initial conditions. A constant value of friction factor corresponding to the initial steady state flow conditions is assumed to be applicable to the transient calculations. For the boundary conditions, at the inlet of the pipeline, the gas density (or pressure) is held constant, while at the outlet of the pipeline the gas mass flux varies with a 24 h cycle, corresponding to changes in consumer demand within a day (Figure 12). The same problem has also been simulated by Taylor *et al.* [4]. In their study, they neglected the inertia term in the momentum equation, and the method of characteristics (MOC) was used to solve the resulting set of linear hyperbolic partial differential equations.

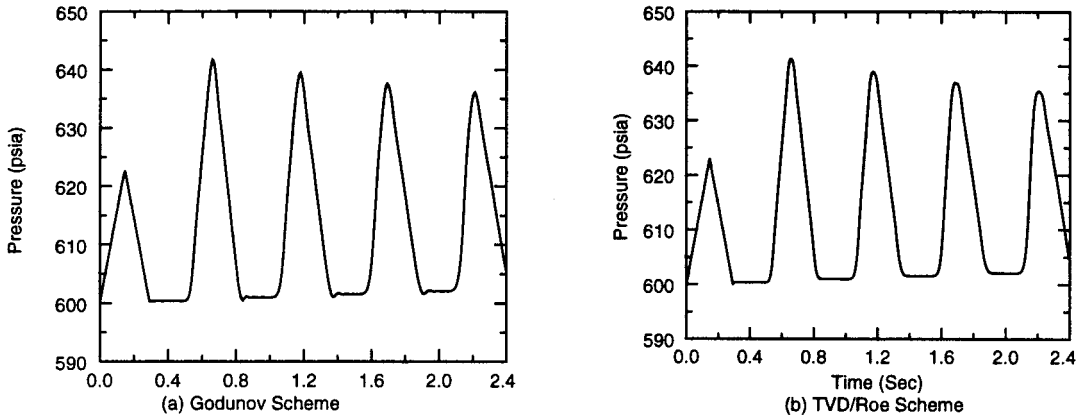

Figure 10. Inset of predicted pressure histories at the inlet for test problem 2 (early time).

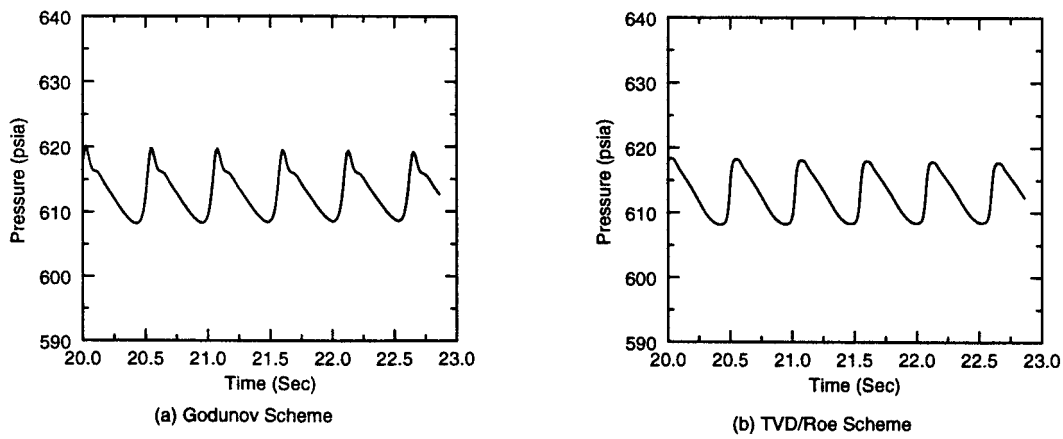

Figure 11. Inset of predicted pressure histories at the inlet for test problem 2 (late time).

Table I is a summary of numerical experiments carried out for the slow transient propagation in this pipeline. In the table, *nj* is the number of total mesh cells, *nk* is the total time steps needed for the computation of a 24 h cycle, Δx is the grid size, Δt is the time step, γ is the CFL-like restriction and τ is the time at which the numerical computation begins to blow up.

Table I demonstrates that the larger grid sizes require smaller CFL-like restriction γ for stable numerical computations, and vice versa; hence, with the decreasing grid size Δx, the stability region of the TVD/Roe scheme is expanded. Similarly, with decreasing time step Δt, while keeping the same grid size Δx, the time at which the numerical computation begins to become unstable increases.

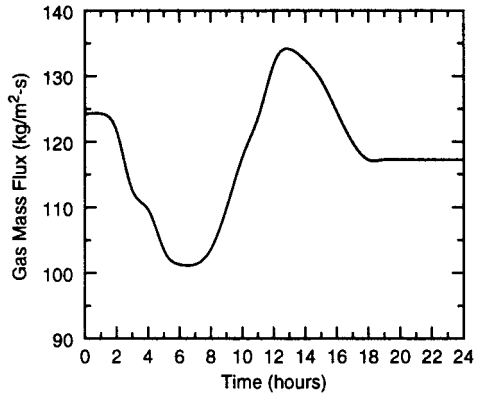

Figure 12. Imposed outlet mass flux.

Table I. Summary of numerical experiments

nj	*nk*	Δx (m)	Δt (ms)	γ	Result
2000	1 196 000	36.13	72.26	0.736	Stable
2000	2 392 000	36.13	36.13	0.368	Stable
2000	23 920 000	36.13	3.613	0.0368	Stable
1000	598 000	72.26	144.52	0.736	Blow up at $\tau = 15.22$ h
1000	1 196 000	72.26	72.26	0.368	Stable
1000	3 588 000	72.26	24.087	0.1227	Stable
1000	11 960 000	72.26	7.226	0.0368	Stable
500	1 495 000	144.52	57.808	0.1472	Stable
500	2 990 000	144.52	28.904	0.0736	Stable
250	1 495 000	289.04	57.808	0.0736	Stable
100	119 600	722.6	722.6	0.368	Blow up at $\tau = 1.144$ h
100	1 196 000	722.6	72.26	0.0368	Blow up at $\tau = 14.592$ h
100	2 392 000	722.6	36.13	0.0184	Blow up at $\tau = 15.054$ h
100	4 784 000	722.6	18.065	0.0092	Blow up at $\tau = 15.62$ h
100	11 960 000	722.6	7.226	0.00368	Stable

Figure 13 shows the comparisons of the predicted pressure histories at outlet and midpoint, the predicted gas mass flux histories at inlet and midpoint of the pipeline, while using the same grid size $\Delta x = 36.13$ m, different time steps ($\Delta t = 72.26$, 36.13, 3.613 ms), and hence different CFL-like restrictions ($\gamma = 0.736$, 0.368, 0.0368). Figure 14 shows the comparisons of the predicted pressure histories at outlet and midpoint, the predicted gas mass flux histories at inlet and midpoint of the pipeline, while using the same grid size ($\Delta x = 72.26$ m), different time steps ($\Delta t = 72.26$, 24.087, 7.226 ms), and hence different CFL-like restrictions ($\gamma = 0.368$, 0.1227, 0.0368).

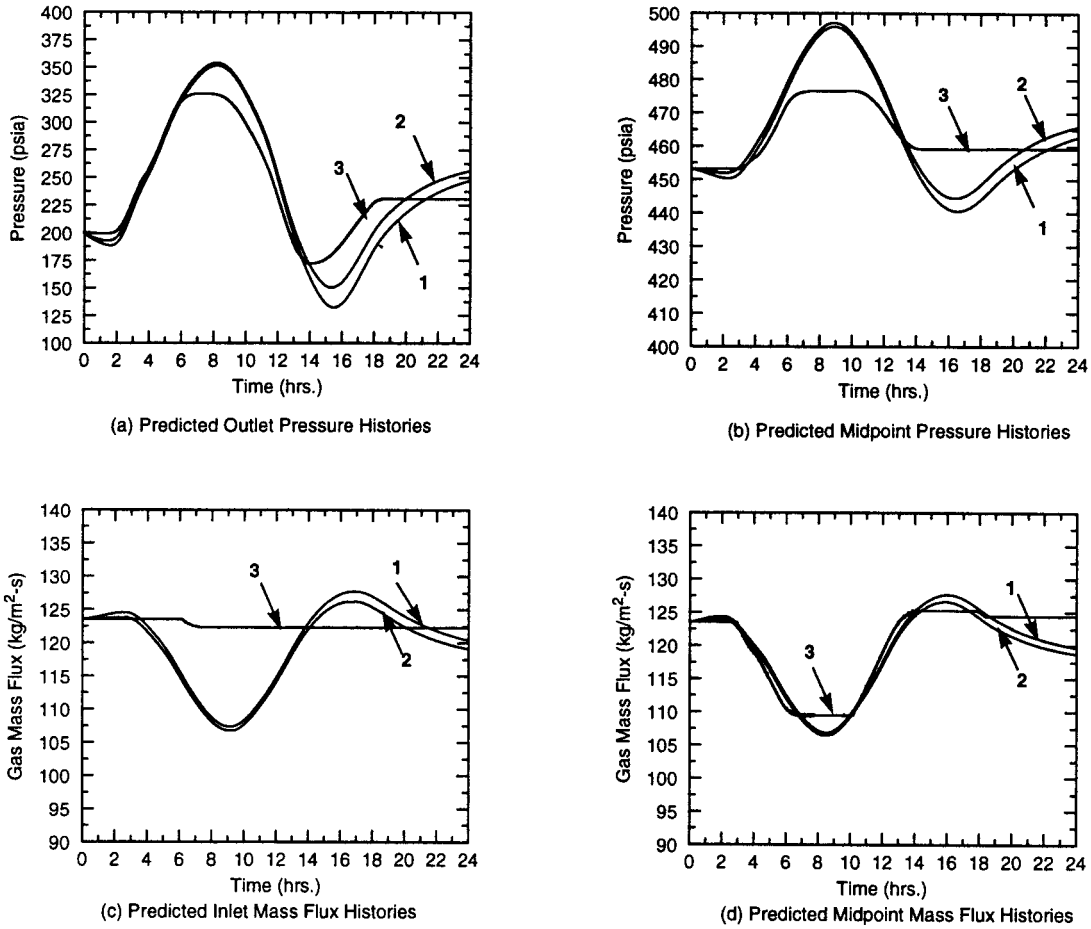

Figure 13. (1) $\Delta x = 36.13$ m, $\Delta t = 72.26$ ms, $\gamma = 0.736$; (2) $\Delta x = 36.13$ m, $\Delta t = 36.13$ ms, $\gamma = 0.368$; (3) $\Delta x = 36.13$ m, $\Delta t = 3.613$ ms, $\gamma = 0.0368$.

Figure 15 shows the comparisons of the predicted pressure histories at outlet and midpoint, the predicted gas mass flux histories at inlet and midpoint of the pipeline, while using the same grid size ($\Delta x = 144.52$ m), different time steps ($\Delta t = 57.808$, 28.904 ms), and hence different CFL-like restrictions ($\gamma = 0.1472$, 0.0736).

Figure 16 shows the comparisons of the predicted pressure histories at outlet and midpoint, the predicted gas mass flux histories at inlet and midpoint of the pipeline, while using the grid size $\Delta x = 289.04$ m, the time step ($\Delta t = 57.808$ ms), and hence the CFL-like restriction ($\gamma = 0.0736$).

Figure 17 shows the comparisons of the predicted pressure histories at outlet and midpoint, the predicted gas mass flux histories at inlet and midpoint of the pipeline, while using the grid size $\Delta x = 722.6$ m, the time step ($\Delta t = 7.226$ ms), and then the CFL-like restriction $\gamma = 0.00368$.

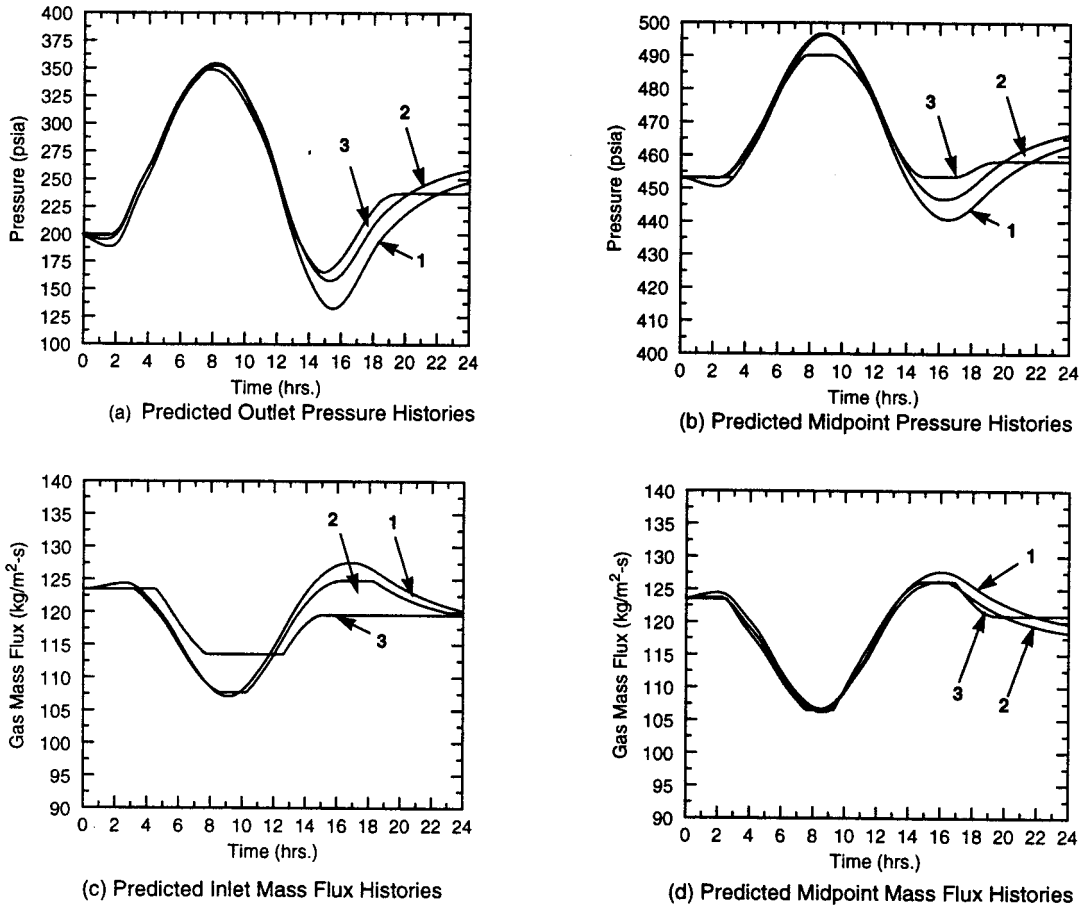

Figure 14. (1) $\Delta x = 72.26$ m, $\Delta t = 72.26$ ms, $\gamma = 0.368$; (2) $\Delta x = 72.26$ m, $\Delta t = 24.087$ ms, $\gamma = 0.1227$; (3) $\Delta x = 72.26$ m, $\Delta t = 7.226$ ms, $\gamma = 0.0368$.

Remark

Harten [17] has proved that his second-order-accurate, 5-point explicit scheme is TVD and convergent in the homogeneous constant coefficients case for all initial data of bounded total variation under the following CFL-like restriction (see Lemma 4.2 and Corollary 4.3 of Harten [17], p. 371).

$$\lambda \max|a^k| \leq \gamma = \min \gamma^k \leq 1, \tag{73}$$

where $\lambda = \Delta t/\Delta x$, a^k is the eigenvalue of the Jacobian matrix at some averaged state [defined by Equations (20) and (21)]. In the present study, Roe's linearization technique is used, and a^k

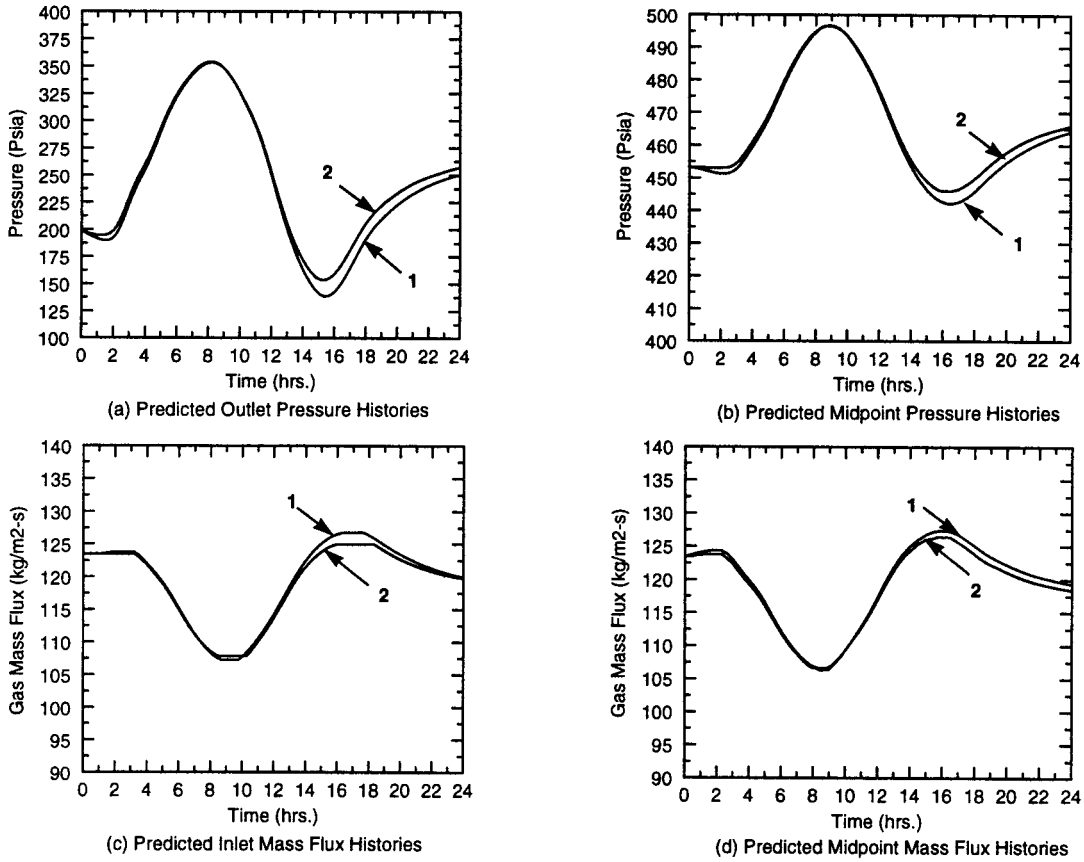

Figure 15. (1) $\Delta x = 144.52$ m, $\Delta t = 57.808$ ms, $\gamma = 0.1472$; (2) $\Delta x = 144.52$ m, $\Delta t = 28.904$ ms, $\gamma = 0.0736$.

in Equation (73) is calculated by Equation (35). Hence, for the calculations of our inhomogeneous system of non-linear hyperbolic conservation laws (Equation (7))

$$\gamma = \lambda \max|c + \bar{u}|, \tag{74}$$

where c is the isothermal acoustic speed in the gas, and $\bar{u}$ is the Roe-averaged velocity [see Equation (34)].

The numerical experiments (see Table I) have demonstrated that the CFL-like restriction γ that guarantees the TVD of the scheme and convergence in the homogeneous constant coefficient case [i.e. $A(U) \equiv (\partial/\partial U)f(U) = \text{constant}$ in Equation (19)] cannot guarantee even the non-linear stability for the present inhomogeneous system of non-linear hyperbolic conservation laws (Equation (7)).

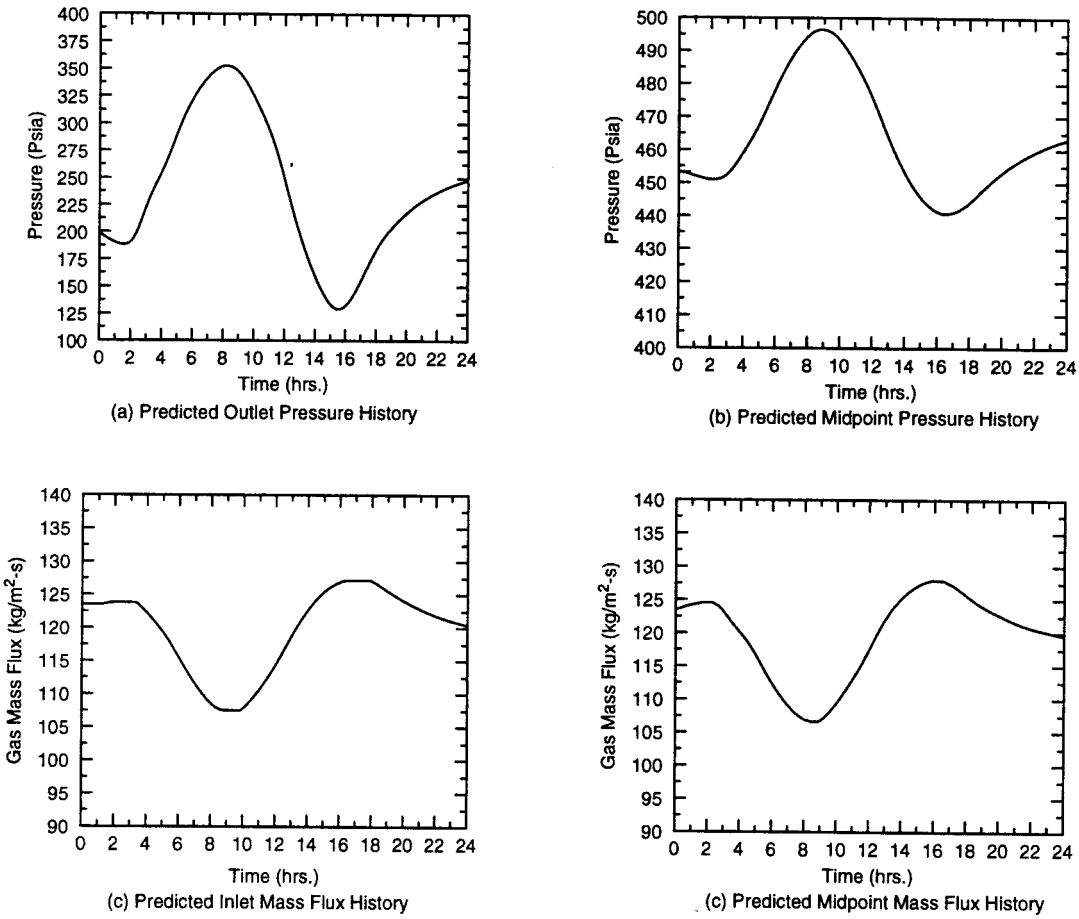

Figure 16. $\Delta x = 289.04$ m, $\Delta t = 57.808$, $\gamma = 0.0736$.

7. CONCLUSIONS

A new class of high-resolution hybrid TVD schemes, with appropriate boundary condition handling capability, is proposed. These include a hybrid TVD/Godunov scheme, a hybrid TVD/Roe scheme and a hybrid TVD/LW scheme. These hybrid TVD schemes enable us to achieve a higher resolution capturing of transients propagation that help to eliminate the frontal oscillations and smearing. A severe condition, involving instantaneous downstream valve closure was used to test the efficacy of these hybrid TVD schemes. In spite of the strong wave generated, these hybrid TVD schemes successfully handled the problem. The results generated by the hybrid TVD/Roe and TVD/Godunov schemes are excellent and comparable with each other, and the hybrid TVD/LW scheme performed reasonably well. The efficacy of different numerical boundary condition treatment strategies is also investigated.

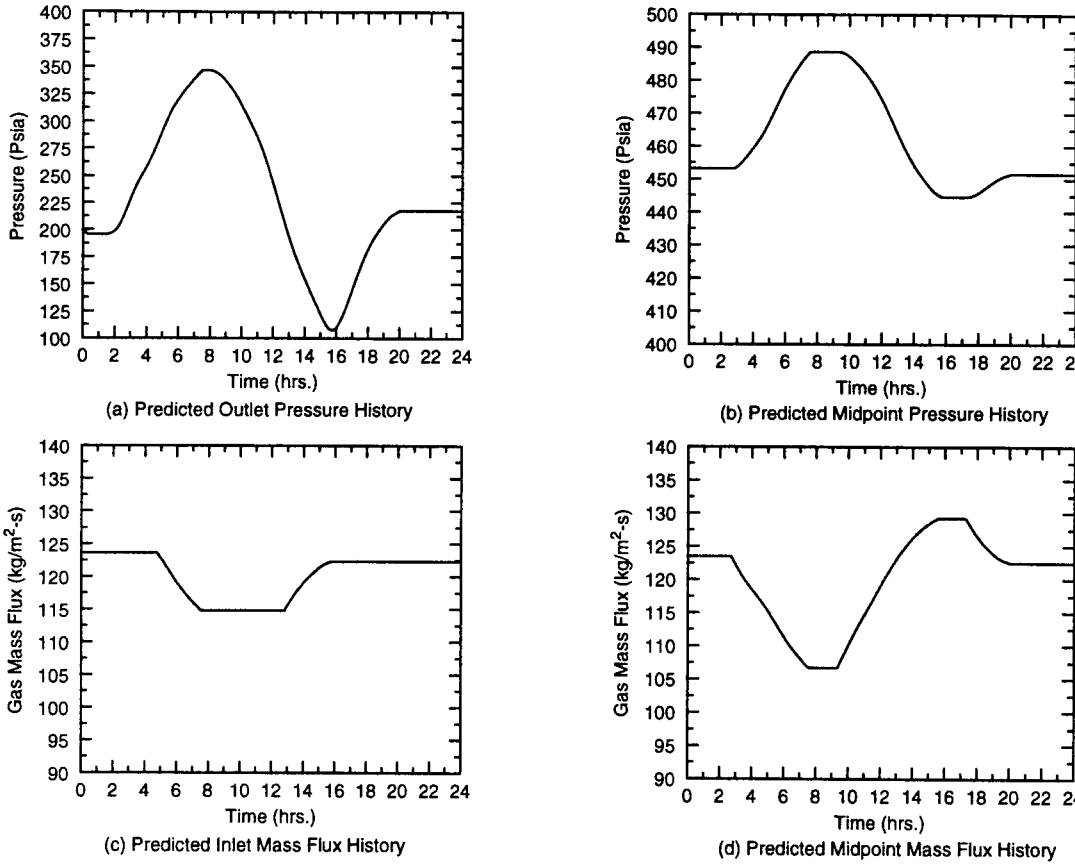

Figure 17. $\Delta x = 722.6$ m, $\Delta t = 7.226$ ms, $\gamma = 0.00368$.

The hybrid TVD/Roe scheme was used to simulate a fast transient in a short pipe. It achieves excellent results that capture and maintain the integrity of the wave fronts even after a long time. For the simulation of a slow transients propagation in a long transmission pipeline by the hybrid TVD/Roe scheme, comparisons of computational results are made using different discretizing parameters. Also, the numerical non-linear stability problem is briefly discussed, while using the hybrid TVD/Roe scheme to solve this mixed initial boundary value problem of a non-homogeneous system of non-linear hyperbolic conservation laws for a long transmission pipeline.

ACKNOWLEDGMENTS

The authors wish to acknowledge the support of this work by the Gas Research Institute (GRI) and Lomic Consultants, Inc.

APPENDIX A. NOMENCLATURE

a^I	eigenvalue of Jacobian matrix $A(U)$ used in Equation (27)
$\tilde{a}^i$	eigenvalue defined by Equation (35)
A	cross-sectional area of pipeline, or the Jacobian matrix
$\tilde{A}$	Jacobian matrix defined by Equation (33)
b	some variable, scalar or vector
c	isothermal speed of sound
D	pipeline diameter
f	flux vector in Equation (19)
$\tilde{f}$	numerical flux vector defined by Equation (25)
f_{g}	friction factor of gas flow
$\vec{F}$	flux vector in Equation (7)
g	gravitational acceleration, or quantity defined by Equation (28)
$\tilde{g}$	defined by Equation (29)
L	left-eigenvector matrix of A used in Equation (23)
m	ρu, gas mass flux
m_0	gas mass flux at the inlet of the pipeline at the beginning of observation
M_{g}	gas molecular weight
p	pressure
Q^k	coefficient of numerical viscosity defined by Equation (40)
$\vec{r}(\vec{U})$	vector in the right-hand side of Equation (7)
R	universal gas constant, or right-eigenvector matrix of A
R^I	right eigenvector used in Equation (22)
$\tilde{R}^i$	right eigenvector defined by Equation (36)
S^k	defined by Equation (28)
t	time
T	absolute gas temperature
u	gas velocity, or state variable vector used in Equations (20) and (21)
$\bar{u}$	Roe-averaged velocity [see Equation (34)]
U	state variable vector in Equation (19)
$\vec{U}$	state variable vector in Equation (7)
v	state variable vector used in Equations (20) and (24)
V	an average function defined by Equations (20) and (21)
x	axial co-ordinate
Z	gas compressibility factor

Greek letters

α	defined by Equation (23)
β	defined by Equation (26)
ε	pipeline roughness
γ	the CFL-like restriction
λ	$\Delta t/\Delta x$

μ gas dynamic viscosity
v defined by Equation (27)
ρ gas density
ρ_0 gas density at the inlet of the pipeline at the beginning of observation
$\bar{\rho}$ $(\rho/\rho_0)^2$ [see Equation (15)]
Υ defined by Equation (30)
ΔL total length, or length from the inlet of pipe to the grid node considered used in Equation (14)
ΔT time interval between two neighboring wave fronts
Δt uniform time step
Δx uniform grid size

Subscripts

g gas
0 inlet, upstream, or initial condition
$i-1$ the $(i-1)$th node of the pipeline
I the ith node of the pipeline
$i+1$ the $(i+1)$th node of the pipeline
$i-3/2$ the midpoint between the $(i-2)$th and $(i-1)$th nodes of the pipeline
$i-1/2$ the midpoint between the $(i-1)$th and ith nodes of the pipeline
$i+1/2$ the midpoint between the ith and $(i+1)$th nodes, or some kind of average between the quantities at ith and $(i+1)$th nodes
$i+3/2$ the midpoint between the $(i+1)$th end $(i+2)$th nodes
nj the njth node, i.e. the outlet or the total mesh number of the pipeline (see Table I)
nk the total time step of calculation (see Table I)
l left side, see Equation (33)
r right side, see Equation (33)

Superscripts

n, $n+1$ the nth and $(n+1)$th time levels respectively

SI metric conversion factors

$\text{ft} \times 3.048\text{E}-01 = \text{m}$
$\text{ft}^3 \times 2.831685\text{E}-02 = \text{m}^3$
$\text{in.} \times 2.54\text{E}+00 = \text{cm}$
$\text{lbm} \times 4.535924\text{E}-01 = \text{kg}$
$\text{miles} \times 1.609344\text{E}+00 = \text{km}$
$\text{psi} \times 6.894757\text{E}+00 = \text{kPa}$
$R(R/1.8) = \text{K}$

Conversion factor is exact.

REFERENCES

1. M.J. Heath and J.C. Blunt, 'Dynamic simulation applied to the design and control of a pipeline network', *J. Inst. Gas Eng.*, **9**, 261–279 (1969).
2. E.B. Wylie, M.A. Stoner and V.L. Streeter, 'Network system transient calculation by implicit methods', *Soc. Pet. Eng. J.*, **3**, 356–362 (1971).
3. V.L. Streeter and E.B. Wylie, 'Natural gas pipeline transients', *Soc. Pet. Eng. J.*, **75**, 357–364 (1970).
4. T.D. Taylor, N.E. Wood and J.E. Power, 'A computer simulation of gas flow in long pipelines', *Soc. Pet. Eng. J. Trans. AIME*, **225**, 297–302 (1962).
5. W. Yow, 'Numerical error in natural gas transient calculations', *ASME Trans. Series D*, **94**, 422–428 (1972).
6. E.B. Wylie, V.L. Streeter and M.A. Stoner, 'Unsteady natural gas calculation in complex piping systems', *Soc. Pet. Eng. J.*, **10**, 35–43 (1974).
7. H.H. Rachford Jr., T. Dupont, 'A fast, highly accurate means of modeling transient flow in gas pipeline systems by variational methods', *Soc. Pet. Eng. J.*, **15**, 165–178 (1974).
8. J.L. Steger and R.F. Warming, 'Flux vector splitting of the inviscid gas dynamic equations with applications to finite-difference methods', *J. Comput. Phys.*, **40**, 263 (1981).
9. R. Courant, E. Isaacson and M. Rees, 'On the solution of nonlinear hyperbolic differential equations by finite differences', *Commun. Pure Appl. Math.*, **5**, 243 (1952).
10. P.D. Lax and B. Wendroff, 'Systems of conservation laws', *Commun. Pure Appl. Math.*, **13**, 217–237 (1960).
11. R.W. MacCormack, 'The effects of viscosity in hypervelocity impact cratering', *AIAA Paper 69-354*, 1969.
12. G.A. Sod, 'A survey of several finite difference methods for systems of non-linear hyperbolic conservation laws', *J. Comput. Phys.*, **27**, 1–35 (1984).
13. J. Von Neumann and R.D. Richtrnyer, 'A method for the numerical calculation of hydrodynamic shocks', *J. Appl. Phys.*, **21**, 232–237 (1950).
14. J.P. Boris and D.L. Book, 'Flux corrected transport I. SHASTA, a fluid transport algorithm that works', *J. Comput. Phys.*, **11**, 38–69 (1973).
15. B. Van Leer, 'Towards the ultimate conservative difference scheme II. Monotonicity and conservation combined in a second-order scheme', *J. Comput. Phys.*, **14**, 361–370 (1974).
16. P.K. Sweby, 'High resolution schemes using flux limiters for hyperbolic conservation laws', *SIAM J. Numer. Anal.*, **21**, 995–1011 (1984).
17. A. Harten, 'High resolution schemes for hyperbolic conservation laws', *J. Comput. Phys.*, **49**, 357–392 (1983).
18. A. Harten, 'On a class of high resolution total variation stable finite difference schemes', *SIAM J. Numer. Anal.*, **21**, 1–23 (1984).
19. S.K. Godunov, 'Difference method for the numerical computation of discontinuous solutions of equations of hydrodynamics', *Mater. Sbornik, N.S.*, **47**, 271–306 (1959).
20. N.H. Chen, 'An explicit equation for friction factor in pipe', *Ind. Eng. Chem. Fund.*, **15**, 296–297 (1979).
21. P.M. Dranchuk and J.H. Abou-Kassem, 'Calculation of Z factor for natural gases using equations of state', *J. Can. Pet. Technol.*, **15**, 34–36 (1975).
22. C. Hirsch, *Numerical Computation of Internal and External Flows*, *Volume 2: Computational Methods for Inviscid and Viscous Flows*, Wiley, New York, 1990, Chapters 16 and 19.
23. J. Zhou and M.A. Adewumi, 'The development and testing of a new flow equation', *Proc. PSIG (Pipeline Simulation Interest Group) 27th Annual Meeting*, Albuquerque, NM, 19–20 October 1995.
24. R.J. LeVeque and H.C. Yee, 'A study of numerical methods for hyperbolic conservation laws with stiff source terms', *J. Comput. Phys.*, **86**, 187–210 (1990).
25. P.L. Roe, 'Approximate Riemann solvers, parameter vectors and difference schemes', *J. Comput. Phys.*, **43**, 357–372 (1981).
26. R.J. LeVeque, *Numerical Methods for Conservation Laws*, Birkhauser, Basel, 1990, pp. 156–157.
27. H.C. Yee, R.F. Warming and A. Harten, 'On the application and extension of Harten's high-resolution scheme', *NASA 82-28063*, June 1982.
28. C.K. Chu and A. Sereny, 'Boundary conditions in finite difference fluid dynamic codes', *J. Comput. Phys.*, **15**, 476–491 (1974).
29. A.R. Mitchell and D.F. Griffiths, *The Finite Difference Method in Partial Differential Equations*, Wiley, New York, 1980, pp. 190–191.
30. R.M. Beam and R.F. Warming, 'An implicit finite-difference algorithm for hyperbolic systems in conservative-law form', *J. Comput. Phys.*, **22**, 87–110 (1976).
31. A. Sundstrom, 'Note on the paper boundary conditions in finite difference fluid dynamic codes by C.K. Chu and A. Sereny', *J. Comput. Phys.*, **17**, 450–454 (1975).

